MIT Libraries | DSpace@MIT

MIT Open Access Articles

Structural Anomalies and Electronic Properties of an Ionic Liquid under Nanoscale Confinement

The MIT Faculty has made this article openly available. ***Please share*** how this access benefits you. Your story matters.

Citation: Pham, Tuan Anh, Coulthard, Riley M, Zobel, Mirijam, Maiti, Amitesh, Buchsbaum, Steven F et al. 2020. "Structural Anomalies and Electronic Properties of an Ionic Liquid under Nanoscale Confinement." Journal of Physical Chemistry Letters, 11 (15).

As Published: 10.1021/ACS.JPCLETT.0C01810

Publisher: American Chemical Society (ACS)

Persistent URL: https://hdl.handle.net/1721.1/133065

Version: Author's final manuscript: final author's manuscript post peer review, without publisher's formatting or copy editing

Terms of use: Creative Commons Attribution-Noncommercial-Share Alike

Massachusetts Institute of Technology

Disclaimer

This document was prepared as an account of work sponsored by an agency of the United States government. Neither the United States government nor Lawrence Livermore National Security, LLC, nor any of their employees makes any warranty, expressed or implied, or assumes any legal liability or responsibility for the accuracy, completeness, or usefulness of any information, apparatus, product, or process disclosed, or represents that its use would not infringe privately owned rights. Reference herein to any specific commercial product, process, or service by trade name, trademark, manufacturer, or otherwise does not necessarily constitute or imply its endorsement, recommendation, or favoring by the United States government or Lawrence Livermore National Security, LLC. The views and opinions of authors expressed herein do not necessarily state or reflect those of the United States government or Lawrence Livermore National Security, LLC, and shall not be used for advertising or product endorsement purposes.

Structural anomalies and electronic properties of an ionic liquid under nanoscale confinement

*Tuan Anh Pham,[1,†] Riley M. Coulthard,[1,2] Mirijam Zobel,[3] Amitesh Maiti,[1] Steven F. Buchsbaum,[1] Colin Loeb,[1] Patrick G. Campbell,[1] Desirée L. Plata,[4] Brandon C. Wood,[1] Francesco Fornasiero,[1] Eric R. Meshot[1,]**

[1]Physical and Life Sciences Directorate, Lawrence Livermore National Laboratory

Livermore, California USA

[2]Department of Chemical and Environmental Engineering, Yale University, New Haven, Connecticut USA

[3]Department of Chemistry, University of Bayreuth, Bayreuth, Germany

[4]Department of Civil and Environmental Engineering, MIT, Cambridge, Massachusetts USA

[†]Corresponding author email: pham16@llnl.gov

*Corresponding author email: meshot1@llnl.gov

ABSTRACT

Ionic liquids promise far greater electrochemical performance compared to aqueous systems, yet key physicochemical properties governing their assembly at interfaces within commonly used graphitic nanopores remain poorly understood. In this work, we combine synchrotron X-ray scattering with first-principles molecular dynamics simulations to unravel key structural characteristics of 1-alkyl-3-methylimidazolium bis(trifluoromethylsulfonyl)imide ($[TFSI]^-$) ionic liquids confined in carbon slit pores. X-ray scattering reveals selective pore filling due to size exclusion, while filled pores exhibit disruption in IL intermolecular structure, the extent of which increases for narrower slit pores. First-principles simulations corroborate this finding and quantitatively describe how perturbations in the local IL structure, particularly the hydrogen-bond network, depend strongly on the degree of confinement. Despite significant deviations in structure under confinement, electrochemical stability remains intact, which is important for energy storage based on nanoporous carbon electrodes (e.g., supercapacitors).

Due to a suite of attractive and widely tunable physiochemical properties, room-temperature ionic liquids (ILs) have emerged as highly promising electrolytes in a wide range of technologies, including catalysis,[1] ion batteries,[2] CO_2 capture,[3] electrodeposition,[4-6] and supercapacitors.[7, 8] Both experimental and computational studies highlighted that understanding the detailed structure and arrangement of ions in porous electrodes is essential for optimizing performance for many of these applications.[9-11] A prime example by Chmiola, et al.[12] indicated that an optimal capacitance is achieved when ion size matched that of the pore, which was attributed to distortion of the ion solvation under spatial confinement.[13, 14] However, since this initial discovery, detailed and comprehensive structural insights have been slow to evolve because electrolyte behavior at interfaces and under confinement is challenging to resolve. These characteristics are especially intractable for emergent electrolytes like ILs that exhibit bulky, flexible, and widely varying molecular configurations. Therefore, detailed understanding of IL desolvation and its dependence on the degree of ion confinement remains largely lacking.

Among X-ray reflectivity,[15] X-ray spectroscopy,[16, 17] neutron scattering,[18] AFM,[19] vibrational spectroscopy,[20] and nuclear magnetic resonance (NMR),[2, 21] X-ray scattering has become a particularly prominent tool for investigating interfacial and confined IL structure because it is a rapid, non-destructive, and multiscale probe. Recent X-ray scattering experiments have made important progress toward deciphering the complex nature of ions under confinement within carbon pores, including aqueous salts[22] and ILs.[23-25] These studies have led to some consensus that structural deviations from bulk such as densification of the electrolyte may manifest under confinement,[24] if only locally near the interface.[10, 19, 26] For instance, landmark results by Futamura, et al.[23] recently provided evidence that the Coulombic ordering between neighboring ions may be partially disrupted in narrow carbon pores of 1 nm and below in width.

Classical theory aided in interpreting or validating data from these experiments, while many additional independent simulations were geared toward elucidating IL behavior at nanocarbon interfaces.[27] For example, molecular dynamics (MD) simulations indicated that an IL can spontaneously fill nanometer-wide carbon pores and consequently exhibits a partial decrease in ion coordination even in the absence of a bias potential.[28, 29] Classical MD simulations and density functional theory (DFT) calculations also made exciting predictions that the capacitance of IL-filled carbon pores may oscillate as a function of pore size.[30-32] However, despite extensive experimental and theoretical studies, there remain several unresolved mechanistic details regarding the structural dependence on relative pore-ion size matching and confinement effects on both hydrogen bonding and electrochemical stability.

In this work, we employed synchrotron X-ray scattering and MD simulations to investigate confinement effects on the structural and electronic properties of a common class of ILs – 1-alkyl-3-methylimidazolium cations paired with a bis(trifluoromethylsulfonyl)imide anion $[TFSI]^-$ (Figure 1a). Rather than relying on classical force fields that are biased by specific parameterization, we employed first-principles MD (FPMD) simulations devoid of *a priori* assumptions. We directly cross-validated the bulk structure of the IL obtained from experiments and FPMD simulations as a baseline before corroborating the diminishing longer range order caused by increasing confinement. Comparing the relative size d of ions and pores reveals selective pore filling due to size exclusion ($d_{ion} \gtrsim d_{pore}$), while the degree of IL disorder in filled pores exhibits a clear dependence as ions approach the hard confinement limit ($d_{ion} = d_{pore}$). FPMD simulations provide a mechanistic understanding of how the experimentally observed disorder of the IL is exacerbated in cases of stronger confinement. We found that ion desolvation is fundamentally governed by destruction of the IL hydrogen-bond network due to

extreme proximity of the hydrophobic pore walls, which manifests in under-coordinated ions. Despite drastic physical changes in the IL ordering, the electrochemical window is interestingly unaltered in narrow carbon pores. This suggests the electrochemical stability remains intact under confinement, which is important for energy storage based on nanoporous carbon electrodes.

To probe ILs under confinement, we synthesized hierarchical carbon aerogel monoliths[33] with tuned pore size distributions. We activated resorcinol-formaldehyde-derived carbon aerogels at 950 °C for times ranging from 5-240 min under CO_2 flow to etch slit pores into the sidewalls of native macropores (Figure 1b, S1)[34, 35] and achieve activation levels of 5-54 % (i.e., mass loss relative to the unactivated aerogel). Supplemental X-ray scattering and Raman spectroscopy together indicate that the surface structure of the pores that interfaces with the IL is unchanged with activation (Figure S2). The IL was loaded into aerogels under a low-vacuum bake to remove moisture and ensure maximal wetting of the pores before sealing the combined materials in capillaries for X-ray analysis. We analyzed the confined structure by comparing X-ray scattering peak intensities from the bulk IL material versus IL loaded in carbon aerogels that have synthetically tuned pore sizes (Figure 1b, S3).

Following the approach presented in previous studies,[23, 25] we assumed the total scattering from IL-wetted aerogels $I(q)_{total}$ is the summation of contributions from the aerogel, bulk IL, and the confined IL, or $I(q)_{total} = I(q)_{aerogel} + I(q)_{bulk} + I(q)_{confined}$ (Figure S4). Thus, recording peak intensity shifts after subtracting the aerogel contribution $I(q)_{aerogel}$ from $I(q)_{total}$ provides a quantitative description of the degree to which IL order deviates from the bulk structure. Note that $I(q)_{bulk}$ signal persists due to IL residue around outer surfaces of the aerogel as well as in large macropores, so our reported values from $I(q)_{total} - I(q)_{aerogel}$ represent lower bounds on the

degree of disorder. Characteristic peaks near q = 1.5 Å^{-1} and 0.9 Å^{-1} are known to be related to separation distances between unlike ions (i.e., cation-anion) and like ions (cation-cation or anion-anion), respectively.[36] Accordingly, the significant decrease in the low-q peak intensity indicates that the longer-range order of the ions inside the aerogels is disrupted (Figure 1c). Normalizing X-ray peak intensity by the aerogel's specific surface area reveals a trend across activation levels that is not constant (Figure S6). Although this does not exclude contributions due to interfacial liquid structure, the increased aerogel surface area with activation alone cannot explain the observed X-ray signal changes. This reinforces the notion that the peak attenuation is a signature of ion solvation distortions characteristic of confinement.

Coupling this X-ray analysis with high-resolution porosimetry provides insight into the pore filling and desolvation as cation size, d_{ion}, is tuned via the alkyl chain length. The compromised long-range order of the ILs is readily detected in the high activation aerogels because the ions seem to fill pores that are both larger and more abundant (i.e., d_{pore} ~ 10-20 Å). Considering their dimensions, all ions tested here are expected to fit inside pores of this size regime, which accounts for 38% of the pore volume versus only 12% at low activations (Figure S3). Importantly, the degree to which IL order is reconfigured increases with d_{ion}, which is consistent with a mechanism of desolvation driven by spatial confinement. However, this trend with d_{ion} is reversed at low activation due to size exclusion from pores under ~10 Å, as illustrated in the inset of Figure 1d. In particular, tuning d_{ion} revealed evidence of selective pore filling based on size (Figure 1d). We expect cations containing butyl or dodecyl chains to experience larger energy penalties to enter the narrowest pores that dominate the aerogel's volume at low activation (i.e., 87% pore volume has $d_{pore} \lesssim$ 10 Å). Therefore, pores in this size regime are not efficiently filled, and the corresponding I(q) signals are closer to those of the bulk IL.

To decipher detailed IL structure within these pores, we first directly cross-validated X-ray measurements with FPMD simulations in the bulk phase (Figure S8). This quantitative comparison validates that our simulations properly describe both the intramolecular (r < 4 Å) and intermolecular (r > 4 Å) structure of the IL. Thus, we implicitly capture the electrostatic interactions among ions, which we relate to key regions of excess/depleted charge distribution (Figure 1a). The spatial distribution function (SDF) of anion O atoms around the cation (Figure 2a) illustrates the preferential interaction between cation and anion at specific hydrogen sites around the imidazolium ring (at ~ 2.3 Å separation distance). The hydrogen associated with the carbon atom in between the two nitrogens (H3) is acidic[37, 38] and exhibits the strongest hydrogen bonding with anions (Figure S9).[39] Specifically, our simulations predict anion density enrichment around the H3 atom to be 2× compared to the methyl and ethyl groups and 23% greater than the other imidazolium hydrogens.

Having validated our simulations of cation-anion interactions in the bulk phase as a baseline, we further probed coordination and structure of ions confined inside slit pores of 11 Å and 17 Å, which correspond to key sizes found in the aerogels. The characteristic accumulation of anions around H3 is still present in these slit pores. However, Figure 2 illustrates how anion enrichment around the cation is markedly lower as we move from the bulk phase to the 17 Å pore and then to the 11 Å pore (O:H3 coordination ratio of 1.87, 1.80, and 1.62, respectively). In fact, the anion is entirely depleted surrounding H2 near the methyl group in the 11 Å case (Figure 2c). This more restricted distribution of anions about the cations may also be reflected in the slight narrowing of the X-ray scattering peak at q = 1.5 Å^{-1} (Figure 1c, S4). Thus, hydrogen bonds are quantifiably and progressively disrupted as confinement conditions escalate (i.e., d_{pore} decreases) in direct connection with the desolvation of ions.

Related to this compromised hydrogen-bonding picture, the extreme proximity of the carbon pore walls restricts the orientational degrees of freedom of the IL molecules. We characterize the orientation of each ion as the angle formed by the cation N-N or anion S-S vector with the normal of the graphene wall (Figure 3a, b). Anion orientations in both pores are largely similar, yet cation orientation in the 11 Å pore exhibits a prominent peak around 45°, which substantially deviates from the peak centered around 90° in the 17 Å pore. The cation prefers a configuration parallel to the graphene wall with a tendency for the acidic H_3 hydrogen to reside in the center of the pore (Figure 3c). However, when d_{pore} limits the IL to a single layer (Figure 3d), the cation orients its less charged methyl and ethyl groups toward the graphene wall. The molecule effectively spans the pore width to balance weak hydrophobic (with wall) and strong Coulombic (with anion) interactions. This illustrates how the proximity of the pore wall locally disrupts the hydrogen bonding and helps explain the depleted region around the H1 hydrogen observed in Figure 2c.

These interactions govern the formation of the single-file organization in the 11 Å pore, with a concentration of anions in the center of the pore and portions of the cations staggered on either side (Figure 3f). Our *ab initio* simulation of cation and anion distributions resembles recent results generated by reverse Monte Carlo simulations and fitting of X-ray data for carbon pores of similar sizes.[23] Interestingly, our simulations predict the closest distance of approach of the ions to the pore wall increases in the narrower 11 Å pore, which is important to consider in supercapacitor design that relies on a 1/distance scaling. While this d_{pore} dependence is in line with trends reported for previous simulations of the same IL across carbon slit pores[23, 40] and free carbon interfaces,[19, 26] we observe comparatively larger separation distances in the smallest pore (Figure S11). This hints at underlying mechanistic details (e.g., confined ion-ion or ion-wall

interactions) implicitly captured in our *ab initio* simulations that may not yet be fully realized in classical frameworks. Another implication of pronounced hydrophobic interactions at the wall and weakened hydrogen bonding is a likely connection to enhanced IL diffusion in carbon pores,[21, 41, 42] which our preliminary simulations suggest should be enhanced proportionally according to ~$1/d_{\text{pore}}$ (not shown).

Despite perturbations in order and hydrogen bonding under confinement, we do not observe significant effects on the electronic properties of the IL, although previously reported links in other liquids between structural changes and electronic characteristics.[43] First, the density of states (DOS) of the graphene-IL interface shows charge transfer is unlikely because the HOMO and LUMO of the IL are positioned > 2 eV from the graphene's Fermi level (Figure S12). This indicates that the interaction between ions and the graphene pore wall is largely weak and hydrophobic in nature, which supports our interpretation of Figure 3. Next, we computed the electrochemical window (ECW) from the difference between the HOMO and LUMO eigenvalues of [EMIM][[TFSI] in the condensed phase at a level of theory defined by the Perdew, Burke, and Ernzerhof (PBE) approximation.[44, 45] We obtained an ECW value of 3.57 ± 0.3 eV in the 11 Å pore, which is comparable to 3.68 ± 0.2 eV calculated for the bulk. Although both values are below experimental reports,[46] as the PBE approximation is known to underestimate the electronic band gap, relative trends are expected to be qualitatively the same as higher levels of theory.[47] Therefore, the electronic structure of the IL, including its ECW as a proxy for operational stability in a potential device, is predicted to be agnostic to interfacial and confinement effects.

To conclude, we combined X-ray scattering and FPMD simulations to quantitatively describe the structural and electronic characteristics of a prototypical IL confined inside

technologically relevant carbon slit pores. We experimentally confirmed significant disruption in the intermolecular correlation between cations and anions depending on relative scaling of d_{pore} and d_{ion}. Evidence suggests that pores below 10 Å are not extensively filled by ions due to size exclusion, while larger pores are filled at the cost of intermolecular order, which is increasingly perturbed for larger d_{ion}. After cross-validating experiments and *ab initio* simulation for bulk IL, we leveraged this simulation framework to explain mechanisms at the root of this compromised order of ILs inside carbon slit pores. The restricted volume and hydrophobic walls drive the rearrangement and orientation of ions, which disrupts hydrogen bonds and leads to desolvation. Structural anomalies are exacerbated in the most extreme single-file confinement conditions (d_{pore} = 11 Å), wherein the cation dramatically flips its orientation by ~45 degrees and anion-cation solvation decays by 13% from the bulk. Despite significant deviations from the bulk physical structure, our theory predicts the electronic structure of the IL under confinement remains unaltered.

Looking forward, our findings offer new fundamental knowledge and implications to boost energy density in future designs of supercapacitors based on nanoporous carbon electrodes and ILs: 1) the structural dependence (e.g., local density, distance from surface) on both d_{pore} and d_{ion} will critically affect the optimal capacitance; 2) the high ECW of ILs is insensitive to confinement, which is advantageous for designing electrodes across different d_{pore} while maintaining a single, fixed operating voltage limit; 3) the destruction of hydrogen-bond networks and proximity of hydrophobic pore surfaces may be responsible for the enhanced IL transport reported by others, which would benefit charge and discharge rates of supercapacitors.

ACKNOWLEDGMENT

This work was performed under the auspices of the U.S. Department of Energy by Lawrence Livermore National Laboratory (LLNL) under Contract DE-AC52-07NA27344. Funding was provided by LLNL Laboratory Directed Research and Development (LDRD) Program Grant No. 18-LW-064. Portions of this work were carried out with the support of the Diamond Light Source at Beamline I-15. Beamlines 7.3.3 and 12.2.2 were used at the Advanced Light Source, which is supported by the Office of Science, Office of Basic Energy Sciences, of the U.S. Department of Energy under Contract No. DE-AC02-05CH11231. R.M.C. was supported by the National Science Foundation Graduate Research Fellowship. Computational resources from the LLNL Computing Grand Challenge Program are also gratefully acknowledged. The authors thank Martin Kunz and Eric Schaible for beamline support, as well as Mirco Eckardt and MacCallum Robertson for assistance with X-ray experiments and analysis.

FIGURES

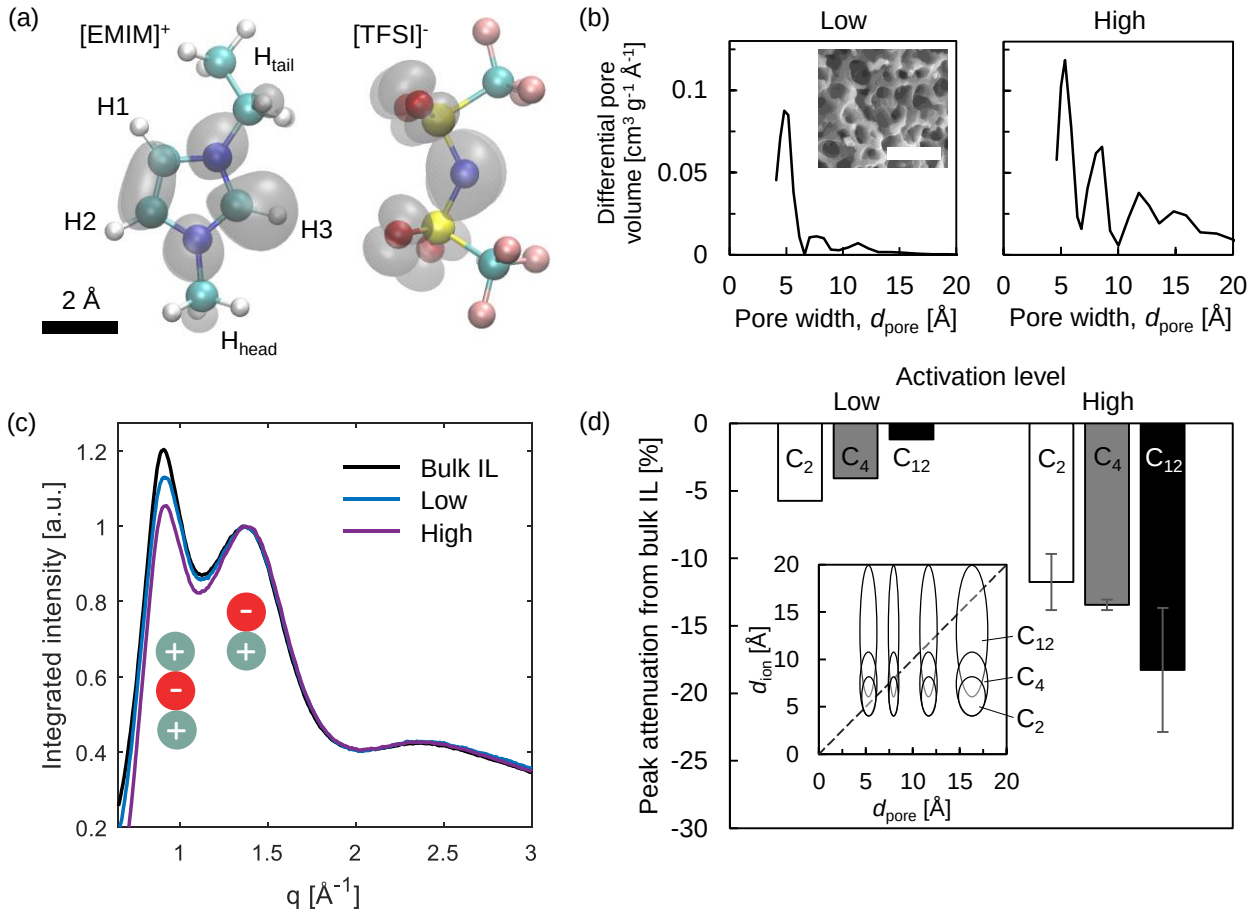

Figure 1. (a) Molecular structures and isosurfaces of electronic charge density associated with the LUMO and HOMO levels of the $[EMIM]^+$ cation and $[TFSI]^-$ anion, respectively. Cyan, blue, white, red, yellow, and pink spheres represent carbon, nitrogen, hydrogen, oxygen, sulfur, and fluorine atoms, respectively. Key hydrogen atoms are labeled for later analysis. A value of 0.02 a.u. was used for the isovalue of the isosurfaces (grey), and the 2 Å scale bar provides reference for ion size. (b) Representative pore size distributions measured by porosimetry for low (5%) and high (35-44%) activation. Inset SEM shows macropore structure of aerogel with low activation (scalebar: 3 μm). (c) Integrated X-ray scattering I(q) data after subtracting the dry aerogel data, as compared with the bulk IL data, for different aerogel activation levels (inset

cartoons depict the specific type ion interaction assigned to each peak). We define $q = 4\pi/\lambda \sin(\theta)$, where λ is the X-ray wavelength and 2θ is the scattering angle, and all measurements were collected and averaged at several locations across millimeters within each sample. (d) Percent difference in peak intensity attenuation from Figure S7 taken at $q = 0.9$ Å^{-1} compared to the bulk IL curve for a set of cation sizes (i.e., alkyl chain lengths denoted by the number of carbon atoms, C_2 = ethyl, C_4 = butyl, C_{12} = dodecyl). Error bars represent standard deviation for replicate samples. Inset plot shows the approximate size ranges of the different cations (*y* axis) versus the measured pore sizes (*x* axis) for high activation with a yellow-green-blue colormap representing pore volume in decreasing order (*z* axis). Oval length equals the range from width to extended length of the cation and oval width equals the range of each major pore size peak in porosimetry. $[TFSI]^-$ size is not explicitly plotted, yet its dimensions closely overlap the C_2 oval. Dashed $d_{ion} = d_{pore}$ line represents the hard confinement limit.

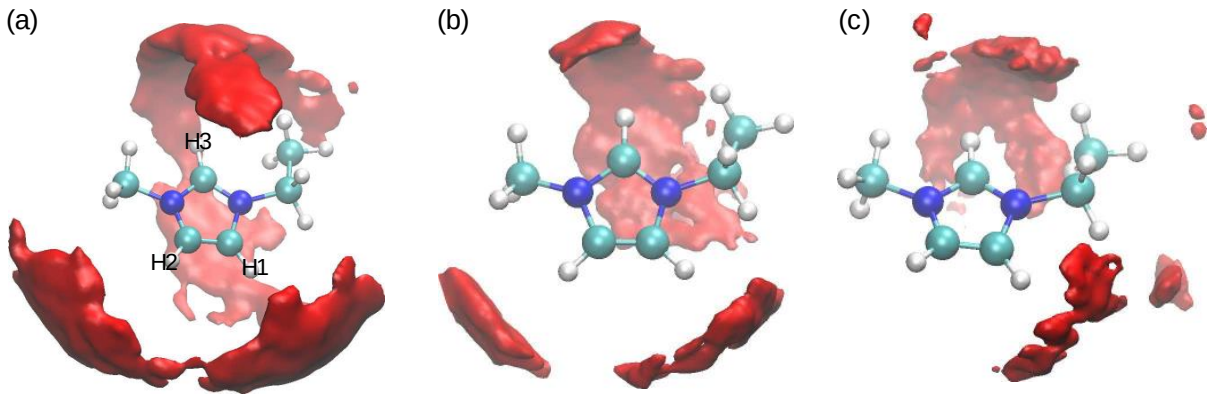

Figure 2: Spatial distribution functions (SDF) at an isovalue of 7.5 atom nm^{-3} showing the accumulation of $[TFSI]^-$ oxygen atoms (red) around the $[EMIM]^+$ cation for both bulk phase (a) and for the confined IL within carbon slit pores with d_{pore} equal to 17 Å (b) and 11 Å (c). Cyan, blue, white, red, yellow, and pink spheres represent carbon, nitrogen, hydrogen, oxygen, sulfur, and fluorine atoms, respectively. MD snapshots of the associated supercells are shown in Figure S10.

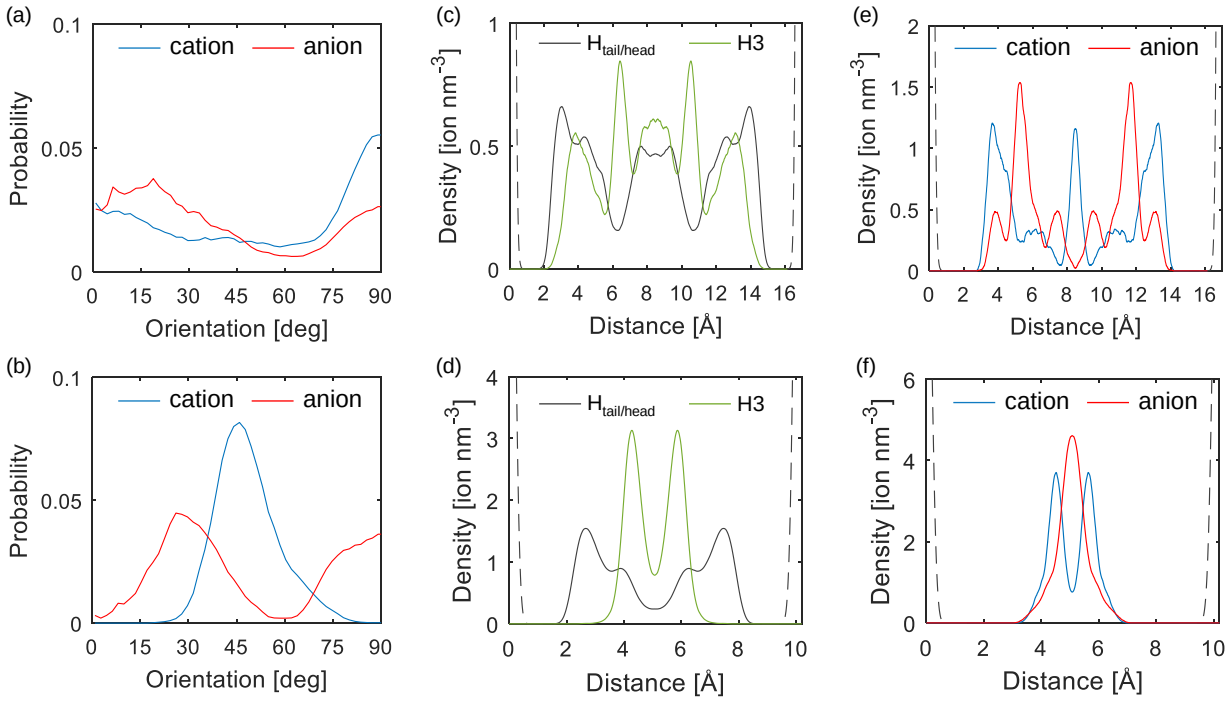

Figure 3. Orientation and density of [EMIM][TFSI] confined within pores of different widths: 17 Å in (a), (c), (e) and 11 Å in (b), (d), (f). (a), (b) Orientation measure by the N-N vector of $[EMIM]^+$ cations and the S-S vector of $[TFSI]^-$ anions with respect to the normal of the graphene wall (i.e., 0 degrees is perpendicular to the wall). Probability calculated by dividing the number of instances per simulation step at each orientation by the total number of instances for the entire simulation. (c), (d) Atomic density distributions for specific hydrogen sites on the $[EMIM]^+$ cation, where H3 is defined as in Figures 1 and 2 and $H_{tail/head}$ indicates hydrogen atoms on the cation's methyl and ethyl groups. (e), (f) Atomic density distributions for the center of mass of the cations and anions. Dashed gray lines represent the density of carbon atoms in the pore wall.

REFERENCES

1. Sheldon, R., Catalytic reactions in ionic liquids. *Chemical Communications* **2001,** (23), 2399-2407.
2. Zhang, S.; Zhang, J.; Zhang, Y.; Deng, Y., Nanoconfined Ionic Liquids. *Chemical Reviews* **2017,** *117* (10), 6755-6833.
3. Zeng, S.; Zhang, X.; Bai, L.; Zhang, X.; Wang, H.; Wang, J.; Bao, D.; Li, M.; Liu, X.; Zhang, S., Ionic-Liquid-Based CO2 Capture Systems: Structure, Interaction and Process. *Chemical Reviews* **2017,** *117* (14), 9625-9673.
4. Abbott, A. P.; McKenzie, K. J., Application of ionic liquids to the electrodeposition of metals. *Physical Chemistry Chemical Physics* **2006,** *8* (37), 4265-4279.
5. Simka, W.; Puszczyk, D.; Nawrat, G., Electrodeposition of metals from non-aqueous solutions. *Electrochimica Acta* **2009,** *54* (23), 5307-5319.
6. Pham, T. A.; Horwood, C.; Maiti, A.; Peters, V.; Bunn, T.; Stadermann, M., Solvation Properties of Silver and Copper Ions in a Room Temperature Ionic Liquid: A First-Principles Study. *The Journal of Physical Chemistry B* **2018,** *122* (50), 12139-12146.
7. Simon, P.; Gogotsi, Y., Materials for electrochemical capacitors. *Nat Mater* **2008,** *7* (11), 845-854.
8. Miller, J. R.; Simon, P., Electrochemical Capacitors for Energy Management. *Science* **2008,** *321* (5889), 651.
9. Forse, A. C.; Merlet, C.; Griffin, J. M.; Grey, C. P., New Perspectives on the Charging Mechanisms of Supercapacitors. *Journal of the American Chemical Society* **2016,** *138* (18), 5731-5744.
10. Fedorov, M. V.; Kornyshev, A. A., Ionic Liquids at Electrified Interfaces. *Chemical Reviews* **2014,** *114* (5), 2978-3036.
11. Salanne, M.; Rotenberg, B.; Naoi, K.; Kaneko, K.; Taberna, P. L.; Grey, C. P.; Dunn, B.; Simon, P., Efficient storage mechanisms for building better supercapacitors. *Nature Energy* **2016,** *1* (6), 16070.
12. Chmiola, J.; Yushin, G.; Gogotsi, Y.; Portet, C.; Simon, P.; Taberna, P. L., Anomalous Increase in Carbon Capacitance at Pore Sizes Less Than 1 Nanometer. *Science* **2006,** *313* (5794), 1760-1763.

13. Largeot, C.; Portet, C.; Chmiola, J.; Taberna, P.-L.; Gogotsi, Y.; Simon, P., Relation between the Ion Size and Pore Size for an Electric Double-Layer Capacitor. *Journal of the American Chemical Society* **2008,** *130* (9), 2730-2731.
14. Chmiola, J.; Largeot, C.; Taberna, P.-L.; Simon, P.; Gogotsi, Y., Desolvation of Ions in Subnanometer Pores and Its Effect on Capacitance and Double-Layer Theory. *Angewandte Chemie International Edition* **2008,** *47* (18), 3392-3395.
15. Mezger, M.; Schröder, H.; Reichert, H.; Schramm, S.; Okasinski, J. S.; Schöder, S.; Honkimäki, V.; Deutsch, M.; Ocko, B. M.; Ralston, J.; Rohwerder, M.; Stratmann, M.; Dosch, H., Molecular Layering of Fluorinated Ionic Liquids at a Charged Sapphire (0001) Surface. *Science* **2008,** *322* (5900), 424-428.
16. Yamada, H.; Ide, N.; Iihara, J., Distortion of Ions in Nanoporous Electrodes Revealed by in Situ X-ray Absorption Spectroscopy. *The Journal of Physical Chemistry C* **2015,** *119* (9), 4736-4741.
17. Buchner, F.; Forster-Tonigold, K.; Kim, J.; Adler, C.; Bansmann, J.; Groß, A.; Behm, R. J., Experimental and Computational Study on the Interaction of an Ionic Liquid Monolayer with Lithium on Pristine and Lithiated Graphite. *The Journal of Physical Chemistry C* **2018,** *122* (33), 18968-18981.
18. Boukhalfa, S.; Gordon, D.; He, L.; Melnichenko, Y. B.; Nitta, N.; Magasinski, A.; Yushin, G., In Situ Small Angle Neutron Scattering Revealing Ion Sorption in Microporous Carbon Electrical Double Layer Capacitors. *ACS Nano* **2014,** *8* (3), 2495-2503.
19. Black, J. M.; Walters, D.; Labuda, A.; Feng, G.; Hillesheim, P. C.; Dai, S.; Cummings, P. T.; Kalinin, S. V.; Proksch, R.; Balke, N., Bias-Dependent Molecular-Level Structure of Electrical Double Layer in Ionic Liquid on Graphite. *Nano Letters* **2013,** *13* (12), 5954-5960.
20. Schernich, S.; Kostyshyn, D.; Wagner, V.; Taccardi, N.; Laurin, M.; Wasserscheid, P.; Libuda, J., Interactions Between the Room-Temperature Ionic Liquid [C2C1Im][OTf] and Pd(111), Well-Ordered Al2O3, and Supported Pd Model Catalysts from IR Spectroscopy. *The Journal of Physical Chemistry C* **2014,** *118* (6), 3188-3193.

21. Berrod, Q.; Ferdeghini, F.; Judeinstein, P.; Genevaz, N.; Ramos, R.; Fournier, A.; Dijon, J.; Ollivier, J.; Rols, S.; Yu, D.; Mole, R. A.; Zanotti, J. M., Enhanced ionic liquid mobility induced by confinement in 1D CNT membranes. *Nanoscale* **2016,** *8* (15), 7845-7848.
22. Prehal, C.; Koczwara, C.; Jäckel, N.; Schreiber, A.; Burian, M.; Amenitsch, H.; Hartmann, M. A.; Presser, V.; Paris, O., Quantification of ion confinement and desolvation in nanoporous carbon supercapacitors with modelling and in situ X-ray scattering. *Nature Energy* **2017,** *2*, 16215.
23. Futamura, R.; Iiyama, T.; Takasaki, Y.; Gogotsi, Y.; Biggs, M. J.; Salanne, M.; Ségalini, J.; Simon, P.; Kaneko, K., Partial breaking of the Coulombic ordering of ionic liquids confined in carbon nanopores. *Nature Materials* **2017,** *16*, 1225.
24. Bañuelos, J. L.; Feng, G.; Fulvio, P. F.; Li, S.; Rother, G.; Dai, S.; Cummings, P. T.; Wesolowski, D. J., Densification of Ionic Liquid Molecules within a Hierarchical Nanoporous Carbon Structure Revealed by Small-Angle Scattering and Molecular Dynamics Simulation. *Chemistry of Materials* **2014,** *26* (2), 1144-1153.
25. Ohba, T.; Chaban, V. V., A Highly Viscous Imidazolium Ionic Liquid inside Carbon Nanotubes. *The Journal of Physical Chemistry B* **2014,** *118* (23), 6234-6240.
26. Zhou, H.; Rouha, M.; Feng, G.; Lee, S. S.; Docherty, H.; Fenter, P.; Cummings, P. T.; Fulvio, P. F.; Dai, S.; McDonough, J.; Presser, V.; Gogotsi, Y., Nanoscale Perturbations of Room Temperature Ionic Liquid Structure at Charged and Uncharged Interfaces. *ACS Nano* **2012,** *6* (11), 9818-9827.
27. Hayes, R.; Warr, G. G.; Atkin, R., Structure and Nanostructure in Ionic Liquids. *Chemical Reviews* **2015,** *115* (13), 6357-6426.
28. Merlet, C.; Rotenberg, B.; Madden, P. A.; Taberna, P.-L.; Simon, P.; Gogotsi, Y.; Salanne, M., On the molecular origin of supercapacitance in nanoporous carbon electrodes. *Nat Mater* **2012,** *11* (4), 306-310.

29. Merlet, C.; Péan, C.; Rotenberg, B.; Madden, P. A.; Daffos, B.; Taberna, P. L.; Simon, P.; Salanne, M., Highly confined ions store charge more efficiently in supercapacitors. *Nat Commun* **2013,** *4*.
30. Feng, G.; Cummings, P. T., Supercapacitor Capacitance Exhibits Oscillatory Behavior as a Function of Nanopore Size. *The Journal of Physical Chemistry Letters* **2011,** *2* (22), 2859-2864.
31. Wu, P.; Huang, J.; Meunier, V.; Sumpter, B. G.; Qiao, R., Complex Capacitance Scaling in Ionic Liquids-Filled Nanopores. *ACS Nano* **2011,** *5* (11), 9044-9051.
32. Jiang, D.-e.; Jin, Z.; Wu, J., Oscillation of Capacitance inside Nanopores. *Nano Letters* **2011,** *11* (12), 5373-5377.
33. Baumann, T. F.; Worsley, M. A.; Han, T. Y.-J.; Satcher, J. H., High surface area carbon aerogel monoliths with hierarchical porosity. *Journal of Non-Crystalline Solids* **2008,** *354* (29), 3513-3515.
34. Biener, J.; Stadermann, M.; Suss, M.; Worsley, M. A.; Biener, M. M.; Rose, K. A.; Baumann, T. F., Advanced carbon aerogels for energy applications. *Energy & Environmental Science* **2011,** *4* (3), 656-667.
35. Suss, M. E.; Baumann, T. F.; Bourcier, W. L.; Spadaccini, C. M.; Rose, K. A.; Santiago, J. G.; Stadermann, M., Capacitive desalination with flow-through electrodes. *Energy & Environmental Science* **2012,** *5* (11), 9511-9519.
36. Shimizu, K.; Bernardes, C. E. S.; Canongia Lopes, J. N., Structure and Aggregation in the 1-Alkyl-3-Methylimidazolium Bis(trifluoromethylsulfonyl)imide Ionic Liquid Homologous Series. *The Journal of Physical Chemistry B* **2014,** *118* (2), 567-576.
37. Bhargava, B. L.; Balasubramanian, S., Intermolecular structure and dynamics in an ionic liquid: A Car–Parrinello molecular dynamics simulation study of 1,3-dimethylimidazolium chloride. *Chemical Physics Letters* **2006,** *417* (4), 486-491.
38. Bhargava, B. L.; Balasubramanian, S., Refined potential model for atomistic simulations of ionic liquid [bmim][PF6]. *The Journal of Chemical Physics* **2007,** *127* (11), 114510.

39. Zhao, W.; Leroy, F.; Heggen, B.; Zahn, S.; Kirchner, B.; Balasubramanian, S.; Müller-Plathe, F., Are There Stable Ion-Pairs in Room-Temperature Ionic Liquids? Molecular Dynamics Simulations of 1-n-Butyl-3-methylimidazolium Hexafluorophosphate. *Journal of the American Chemical Society* **2009,** *131* (43), 15825-15833.
40. Xing, L.; Vatamanu, J.; Borodin, O.; Bedrov, D., On the Atomistic Nature of Capacitance Enhancement Generated by Ionic Liquid Electrolyte Confined in Subnanometer Pores. *The Journal of Physical Chemistry Letters* **2013,** *4* (1), 132-140.
41. He, Y.; Qiao, R.; Vatamanu, J.; Borodin, O.; Bedrov, D.; Huang, J.; Sumpter, B. G., Importance of Ion Packing on the Dynamics of Ionic Liquids during Micropore Charging. *The Journal of Physical Chemistry Letters* **2016,** *7* (1), 36-42.
42. Ghoufi, A.; Szymczyk, A.; Malfreyt, P., Ultrafast diffusion of Ionic Liquids Confined in Carbon Nanotubes. *Scientific Reports* **2016,** *6*, 28518.
43. Pan, D.; Wan, Q.; Galli, G., The refractive index and electronic gap of water and ice increase with increasing pressure. *Nature Communications* **2014,** *5* (1), 3919.
44. Zhang, Y.; Maginn, E. J., A Simple AIMD Approach to Derive Atomic Charges for Condensed Phase Simulation of Ionic Liquids. *The Journal of Physical Chemistry B* **2012,** *116* (33), 10036-10048.
45. Perdew, J. P.; Burke, K.; Ernzerhof, M., Generalized Gradient Approximation Made Simple. *Physical Review Letters* **1996,** *77* (18), 3865-3868.
46. Buzzeo, M. C.; Hardacre, C.; Compton, R. G., Extended Electrochemical Windows Made Accessible by Room Temperature Ionic Liquid/Organic Solvent Electrolyte Systems. *ChemPhysChem* **2006,** *7* (1), 176-180.
47. Ong, S. P.; Andreussi, O.; Wu, Y.; Marzari, N.; Ceder, G., Electrochemical Windows of Room-Temperature Ionic Liquids from Molecular Dynamics and Density Functional Theory Calculations. *Chemistry of Materials* **2011,** *23* (11), 2979-2986.

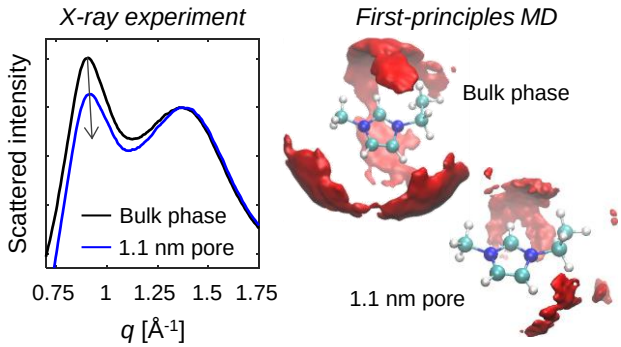

For Table of Contents Only